Effect of a Surface Area and a d-Band Oxidation State on the Activity and Stability of RuO_x Electrocatalysts for Oxygen Evolution Reaction

Tae-Jun Kim,[†,¶] Shin-Ae Park,[†,¶] Seohyoung Chang,[‡] Ho-hwan Chun,[§] and Yong-Tae Kim[†,*]

[†]*School of Mechanical Engineering, Pusan National University, Busan 609-735, Republic of Korea.*
**E-mail: yongtae@pusan.ac.kr*
[‡]*Materials Science Division, Argonne National Laboratory, Argonne, IL, 60439, USA*
[§]*Global Core Research Center for Ships and Offshore Plants (GCRC-SOP), Pusan National University, Busan 609-735, Republic of Korea*
Received February 6, 2015, Accepted March 30, 2015, Published online June 28, 2015

It is widely recognized that RuO_2 is the best electrocatalysts for oxygen evolution reaction (OER) in water splitting in acidic media. In this study, we investigated the effect of a surface area and a d-band oxidation state on the activity and the stability of RuO_x electrocatalysts for OER. We synthesized RuO_x thin film on glassy carbon electrode by the radio frequency magnetic sputtering and controlled the deposition temperature to vary the surface morphology and the electronic structure. In particular, we obtained a precise d-band valence structure by using the synchrotron beam. A higher surface area and a more stable Ru^{4+} state were obtained at a lower deposition temperature owing to a smaller grain size and a lower oxidation state, respectively. As a result, the order of activity and stability is clearly consistent with that of surface area and stable Ru^{4+} state (RuO_x > RuO_x200 > RuO_x400 > RuO_x600). Hence, we suggest that the surface area and the Ru d-band oxidation state should be carefully controlled in the synthesis process in order to enhance the activity and the stability of RuO_x electrocatalysts for OER.

Keywords: Oxygen evolution, RuO_2, Surface area, d-Band

Introduction

The electrolysis for water splitting is of great importance for the sustainable hydrogen production combining with the renewable energy sources like solar or wind power. In the electrolysis, the hydrogen evolution reaction (HER: $4H^+ + 4e^- \rightarrow H_2$) and the oxygen evolution reaction (OER: $2H_2O \rightarrow O_2 + 4H^+ + 4e^-$) occurs at the anode and the cathode, respectively. The most serious hurdle to increase the efficiency of electrolysis is the OER requiring much higher overpotential than the HER to proceed the reaction.[1,2] Most of the efforts for enhancing the performance of electrolyzer have been exerted on the development of better electrocatalysts for OER. Although the electrolysis can be performed in both acidic and alkaline media, there have been more studies in acidic media. This is because the operating current density in acidic media is at least three times higher than that in alkaline media.[3] A drawback of the electrolysis in acidic media in comparison with the alkaline electrolysis is that the noble metal oxides like RuO_2 or IrO_2 should be employed for the OER electrocatalysts, because the anode environment in electrolysis is extremely corrosive. Hence, a lot of studies have focused on how to optimize the electrode structure and to minimize the amount of noble metal used.[4] As it has been widely recognized that RuO_2 is the best electrocatalyst materials for OER in acidic media, many studies to maximize the performance of RuO_2 as OER electrocatalysts have been reported, such as the optimization of sol–gel synthesis process, the size control via wetness method, and the formation of alloy oxide, $RuMO_x$ (M = Pd, Ir, Cu, Co, Re, Cr, Ni).[5–7] Also, the oxygen recombination effect or the synergetic effect has been suggested to elucidate the enhanced activity for OER.[5,6] Nevertheless, as the knowledge on how to design the electrocatalysts is still insufficient, further basic studies is required on how to enhance the activity and the stability of RuO_2 electrocatalysts.

In this study, we intensively investigate the effect of surface area and d-band valence state of RuO_x. In this article, we used RuO_x rather than RuO_2, because the valence of Ru in oxide phase is not exactly 4+ but controlled with the synthetic condition. All the samples were in the shape of thin film and prepared by radio frequency (RF) magnetron sputtering. The morphology and crystal structure of RuO_x catalysts were observed by scanning electron microscopy (SEM) and X-ray diffraction (XRD), respectively. To precisely analyze the d-band valence structure, we employed the high-resolution-X-ray photoemission spectroscopy (HR-XPS) with the synchrotron beam. Electrochemical methods such as rotating disk electrode (RDE) and cyclic voltammetry (CV) were employed to evaluate the OER activity in the acid media.

Experimental

RuO_x thin films were deposited by RF magnetron sputter system (AJA International, Inc., N Scituate, MA, USA) onto

¶ These authors equally contributed to the work.

glassy carbon (GC) disks (5 mm diameter, 5 mm thick). A base pressure of the chamber was 4×10^{-8} Pa. GC disks were polished with 0.05 μm alumina powder (Buehler, IL, USA) on microcloth polishing pads (Buehler), rinsed and sonicated in Millipore water. The RuO_x films were deposited at 25–600 °C and 10 mTorr oxygen partial pressure using a RuO_2 polycrystalline target (AJA International, Inc.). The sputtering deposition was carried with an RF plasma power of 50 W. The quality of films was verified by XPS at Pohang Light Source (PLS). For the X-ray spectroscopy measurements, the RuO_x films were sputtered to the optimal thicknesses, *e.g.*, 10–20 nm. In this study, we used several abbreviations, such as RuO_x, RuO_x200, RuO_x400, and RuO_x600 for RuO_x films deposited at 25, 200, 400, and 600 °C.

The morphology of the sample was observed with Zeiss FE-SEM SUPRA25 and Raith Quantum Elphy in a PNU center for Research facilities. The powder XRD analysis was performed with an advance X-ray diffractometer (D8 ADVANCE, Bruker, WI, USA) with CuK_α radiation ($\lambda = 1.54056$ Å). XRD data were collected over the 2θ range 10–90° with a step size of 0.02° and a counting time of 0.2 s per step. X-ray photoelectron spectroscopy (XPS) analysis was performed with 8A1 beamline in the PLS.

Electrochemical experiments were performed in a three-electrode electrochemical cell with a RDE and a potentiostat (BioLogic VSP, Claix, France) at room temperature. The working electrode was a catalyst-film-covered GC disk (0.19625 cm^2 in area). A Pt wire and a silver/silver chloride (Ag/AgCl) electrode were used as the counter and reference electrodes, respectively. CV were performed in the potential range between 0.05 and 1.2 V (vs. RHE, Reversible hydrogen electrode) in an nitrogen-saturated 0.1 M $HClO_4$ aqueous solution at a scan rate of 50 mV/s. OER measurements were performed in the potential range between 1.2 and 1.8 V (vs. RHE) in an nitrogen-saturated 0.1 M $HClO_4$ aqueous solution at rotation rates of 1600 rpm at a scan rate of 10 mV/s.

Results and Discussion

The surface morphology of prepared samples was, observed with SEM as shown in Figure 1. The aggregate sizes for RuO_x, RuO_x200, RuO_x400, and RuO_x600 were about 5, 20, 50, and 100 nm, respectively. With the deposition temperature, the aggregates size was increased and therefore the surface area was anticipated to be decreased.

The crystal structure was investigated by using the powder XRD techniques and the obtained diffraction patterns were shown in Figure 2 and Figure S1 in Supporting Information. As the GC was used as a substrate of RuO_x deposition, the strong diffraction peak corresponding to the graphite structure was shown in all the obtained diffraction patterns and exactly matched with the index (SG.194, P63/mmC). The peaks at 2θ = 26.5°, 44.5°, 54.6°, and 77.4° are corresponding to graphite (0 0 2), (1 0 1), (0 0 4), and (1 1 0), respectively. In Figure 2, the notable point is that a clear diffraction signal at 2 θ= 35.3° corresponding to the (0 1 1) facet of orthorhombic RuO_2 (SG.58, Pnnm) was shown for all the samples except for RuO_x. This indicates that RuO_x deposited in room temperature is in an amorphous phase or their crystallite size is too small for the diffraction to occur. However, the other samples prepared at above 200 °C have the orthorhombic RuO_2 structure and larger crystallite size. Hence, this result is clearly consistent with the SEM images.

As the morphology and the crystallite structure obviously varied with the deposition condition, we anticipated that the Ru d-band valence structure could also be different from each other. In order to precisely analyze the d-band valence structure, we employed the HR-XPS with the synchrotron beam ($h\nu = 630$ eV). In particular, we intensively measured the valence structure rather than usually employed core level in XPS analysis, because the core level of $Ru3d_{3/2}$ orbital (284.1 eV) is overlapped with the carbon 1s orbital (284.6 eV). As can be seen in Figure S2, the valence structures for the prepared samples are clearly varied with the deposition

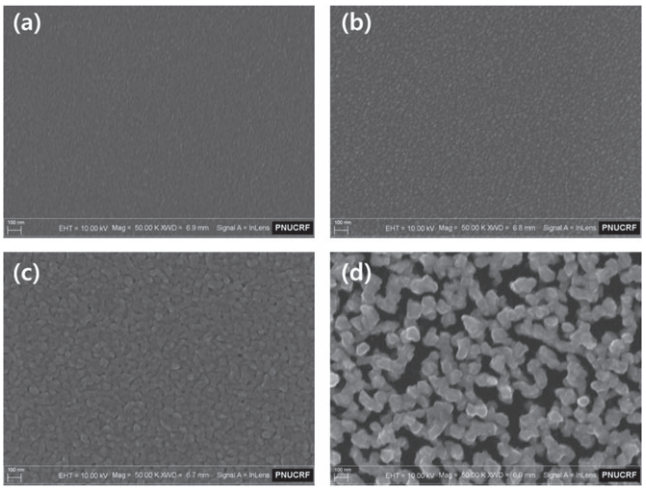

Figure 1. SEM micrographs of RuO_x, RuO_x200, RuO_x400, and RuO_x600.

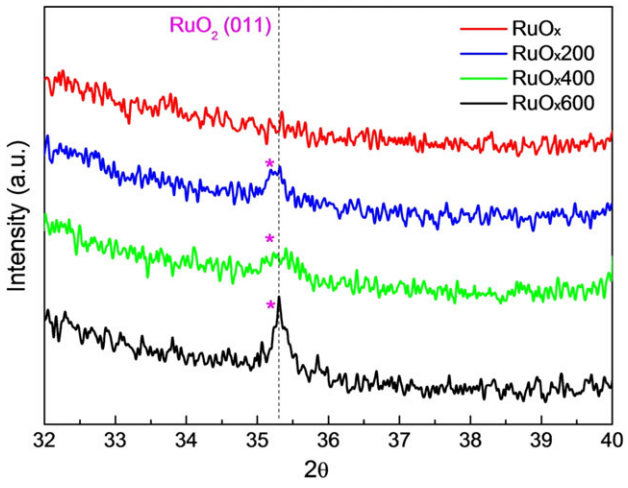

Figure 2. XRD patterns of RuO_x, RuO_x200, RuO_x400, and RuO_x600.

condition. In general, the valence band of RuO_x contains three characteristic peaks corresponding to the Ru–O band originated from the hybridization of Ru 3d and O 2p electrons.[8] The peaks at 6.9, 4.7, and 0.6 eV are corresponding to Ru–Oσ, Ru–Oπ, and Ru–Oπ∗ bond, respectively. Figure 3 shows the magnified Ru valence structure chiefly corresponding to the Ru–Oπ∗ bond. The peak intensity of Ru bulk is the smallest among all the samples, implying that the lower oxidation state represents the smaller valence band near the Fermi level. Hence, the oxidation state of RuO_x is possibly lower than that of RuO_x600.

In order to investigate the electrochemical characteristics of various samples, we carried out the CV. As can be seen in Figure 4(a), a typical shape of cyclic voltammogram of RuO_2 was obtained for all the samples. The electrochemical capacitances including both double layer (non-faradaic) and pseudocapacitance (faradaic) for RuO_x, RuO_x200, RuO_x400, and RuO_x600 were calculated to be 2.62×10^{-5}F, 1.1×10^{-5}F, 3.53×10^{-6}F, and 3.25×10^{-6}F, respectively, implying that the surface area was decreased by increasing the deposition temperature. As exhibited in the SEM images, the decreased surface area is directly attributed to the increased grain size.

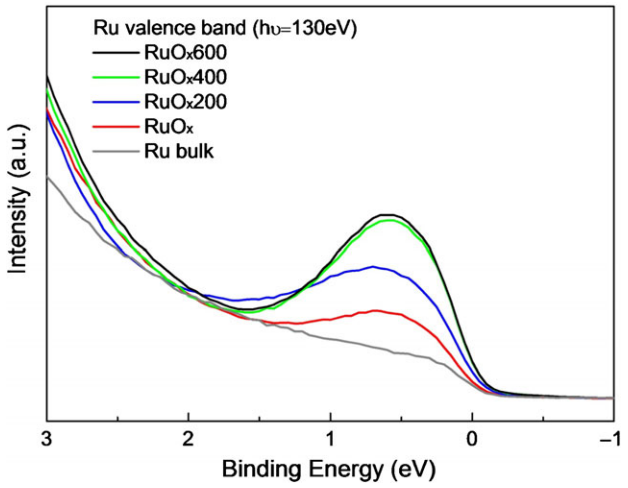

Figure 3. XPS data for valence band of RuO_x, RuO_x200, RuO_x400, RuO_x600 and Ru bulk at $h\nu = 130$ eV.

The OER activity for the various samples was examined by using the RDE technique. As can be seen in Figure 4(b), the order of OER activity expressed by the overpotential at the current density of 10mA/cm^2 was RuO_x (1.54 V) > RuO_x200 (1.60 V) > RuO_x400 (1.64 V) > RuO_x600 (1.73 V), which is same with the order of surface area. This indicates that the OER activity is directly related to the surface area and is consistent with the previous report that the OER activity is governed by the morphological effect rather than the electronic effect.[9]

A notable point in the OER polarization curves is that each sample shows a clearly different change of OER activity after fifth potential cycles. The onset potential for RuO_x was increased from 1.54 to 1.52 V after the potential cycling and that for RuO_x200 was same. However, the OER activity for RuO_x400 and RuO_x600 was decreased from 1.64 and 1.73 V to 1.66 and 1.82 V after the potential cycling, indicating that the order of electrocatalytic stability could be RuO_x > RuO_x200 > RuO_x400 > RuO_x600, same trend with the activity. In a recent study, Markovic *et al*. reported that the valence state of Ru was changed from Ru^{3+} to Ru^{4+} at 1.0 V and from Ru^{4+} to $Ru^{n>4+}$ at about 1.3 V. In particular, it was found that the valence state of $Ru^{n>4+}$ was quite unstable and therefore readily dissolvable.[9] As the valence of RuO_x400 and RuO_x600 is already in Ru^{4+} state, upon applying an anodic potential they are easily dissolved into electrolyte without the oxidation process from Ru^{3+} to Ru^{4+}. On the contrary, because the valence of RuO_x is below Ru^{4+} as confirmed from the XPS results, it initially undergoes the oxidation from Ru^{3+} to Ru^{4+} and therefore the proportion of Ru^{4+} state is more dominant that $Ru^{n>4+}$ at the same condition. Hence, the higher proportion of Ru^{4+} state for RuO_x under applying anodic potential is possibly the origin of enhanced electrocatalytic stability

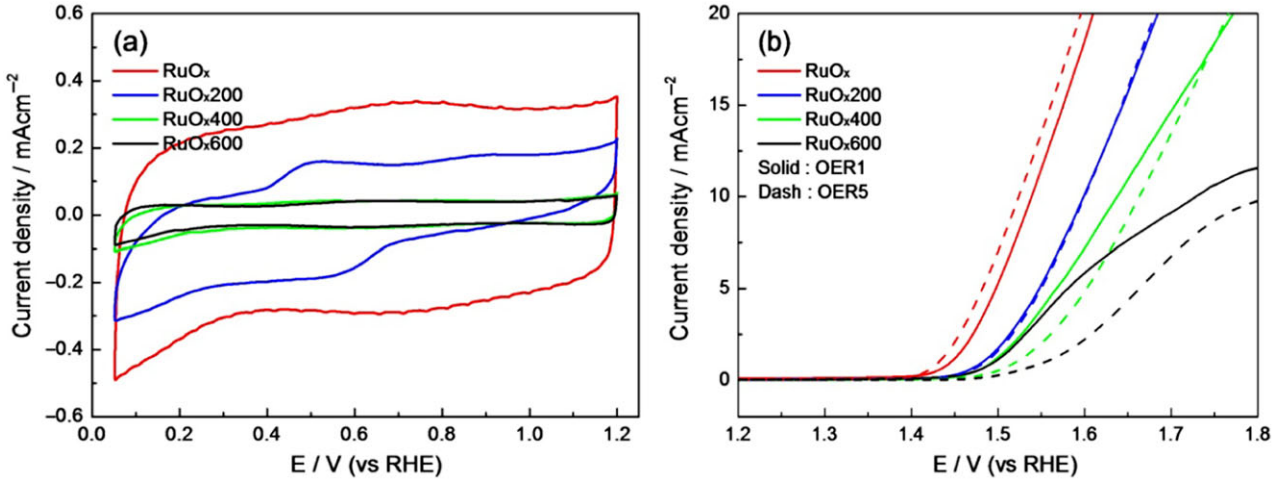

Figure 4. (a) Cyclic voltammetry of RuO_x, RuO_x200, RuO_x400, and RuO_x600 in N_2-purged 0.1 M $HClO_4$ solution at 50 mV/s. (b) Oxygen evolution polarization curves for RuO_x, RuO_x200, RuO_x400, and RuO_x600 at 1600 rpm in N_2-purged 0.1 M $HClO_4$ solution at 10 mV/s.

for OER. Based on the above discussion, we suggest a design rule of OER electrocatalysts that the surface area should be maximized to obtain the enhanced OER activity and the d-band oxidation state should be minimized to increase the electrocatalytic stability.

Conclusion

In this study, we investigated the effect of surface area and d-band oxidation state on the activity and the stability for OER. With the deposition temperature, the grain size of RuO_x was increased, and therefore the surface area was decreased, as confirmed with SEM, XRD, and CV data. Also, the d-band oxidation state was increased with the deposition temperature, as showed in the valence band structure in XPS measurements. It was clearly found that the activity and the stability for OER are directly related to the surface area and the d-band oxidation state, respectively. The order of activity and stability for OER was $RuO_x > RuO_x200 > RuO_x400 > RuO_x600$. In the case of RuO_x, the highest surface area and the lowest d-band oxidation state led to the best performance for OER. Hence, we suggest a design rule for OER electrocatalysts that the surface area should be maximized and the d-band oxidation state should be minimized.

Acknowledgments. This work was supported by the National Research Foundation of Korea (NRF) grant (2012-0008830, NRF-2012-M1A2A2-029543, and 2013M1A8A1040703) and GCRC-SOP funded by the Korea Government (MEST).

Supporting Information. Additional supporting information is available in the online version of this article.

References

1. J. P. Hoare, *The Electrochemistry of Oxygen*, Interscience Publishers, New York, **1968**.
2. R. O'Hayre, *Fuel Cell Fundamentals*, John Wiley & Sons, Hoboken, NJ, **2006**.
3. I. Katsounaros, S. Cherevko, A. R. Zeradjanin, K. J. J. Mayrhofer, *Angew. Chem. Int. Ed.* **2014**, *53*, 102.
4. H. N. Nong, L. Gan, E. Willinger, D. Teschner, P. Strasser, *Chem. Sci.* **2014**, *5*, 2955.
5. J. Jirkovsky, M. Makarova, P. Krtil, *Electrochem. Commun.* **2006**, *8*, 1417.
6. R. Forgie, G. Bugosh, K. C. Neyerlin, Z. Liu, P. Strasser, *Electrochem. Solid-State Lett.* **2010**, *13*, B36.
7. Y. Lee, J. Suntivich, K. J. May, E. E. Perry, Y. Shao-Horn, *J. Phys. Chem. Lett.* **2012**, *3*, 399.
8. J. Riga, C. Tenret-Noel, J. J. Pireaux, R. Caudano, J. J. Verbist, Y. Gobillon, *Phys. Scr.* **1977**, *16*, 351.
9. S. H. Chang, N. Danilovic, K.-C. Chang, R. Subbaraman, A. P. Paulikas, D. D. Fong, M. J. Highland, P. M. Baldo, V. R. Stamenkovic, J. W. Freeland, J. A. Eastman, N. M. Markovic, *Nat. Commun.* **2014**, *5*, 4191.

